

Title	Optimization of annealing conditions to enhance thermoelectric performance of electrodeposited p-type BiSbTe thin films
Authors	Lal, Swatchith;Gautam, Devendraprakash;Razeeb, Kafil M.
Publication date	2019-03-04
Original Citation	Lal, S., Gautam, D. and Razeeb, K.M., 2019. Optimization of annealing conditions to enhance thermoelectric performance of electrodeposited p-type BiSbTe thin films. APL Materials, 7(3), [031102]. DOI:10.1063/1.5049586
Type of publication	Article (peer-reviewed)
Link to publisher's version	https://aip.scitation.org/doi/10.1063/1.5049586 - 10.1063/1.5049586
Rights	© The Author(s) 2019 - https://creativecommons.org/licenses/by/4.0/
Download date	2024-05-13 11:29:54
Item downloaded from	https://hdl.handle.net/10468/9031

Optimization of annealing conditions to enhance thermoelectric performance of electrodeposited p-type BiSbTe thin films

Cite as: APL Mater. 7, 031102 (2019); <https://doi.org/10.1063/1.5049586>

Submitted: 23 July 2018 . Accepted: 10 February 2019 . Published Online: 04 March 2019

Swatchith Lal , Devendraprakash Gautam , and Kafil M. Razeed 



View Online



Export Citation



CrossMark

ARTICLES YOU MAY BE INTERESTED IN

[High-temperature stable refractory nanoneedles with over 99% solar absorptance](#)

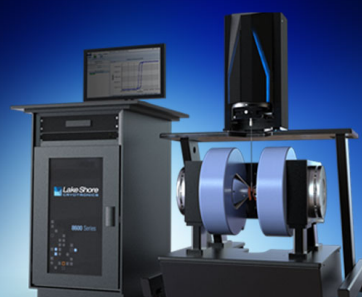
APL Materials **7**, 031101 (2019); <https://doi.org/10.1063/1.5084086>

[Electrolyte-gated magnetoelectric actuation: Phenomenology, materials, mechanisms, and prospective applications](#)

APL Materials **7**, 030701 (2019); <https://doi.org/10.1063/1.5080284>


[Enhanced thermoelectric performance in single-crystal-like semiconducting flexible GaAs films](#)

APL Materials **7**, 031104 (2019); <https://doi.org/10.1063/1.5086061>



8600 Series VSM

For fast, highly sensitive measurement performance

[LEARN MORE](#) 



Optimization of annealing conditions to enhance thermoelectric performance of electrodeposited p-type BiSbTe thin films

Cite as: APL Mater. 7, 031102 (2019); doi: 10.1063/1.5049586

Submitted: 23 July 2018 • Accepted: 10 February 2019 •

Published Online: 4 March 2019



Swatchith Lal, Devendraprakash Gautam,^{a)} and Kafil M. Razeeb^{a)}

AFFILIATIONS

Tyndall National Institute, University College Cork, Dyke Parade, Lee Maltings, Cork T12 R5CP, Ireland

^{a)}Authors to whom correspondence should be addressed: kafil.mahmood@tyndall.ie and d.gautam@tyndall.ie

ABSTRACT

In this work, we report the optimization of annealing process to improve the thermoelectric properties of pulse electrodeposited bismuth antimony telluride (Bi-Sb-Te) films by varying the annealing time-temperature profile. The innovative approach of sandwiched Te in between the Bi-Sb-Te layers aids in compensating the loss of tellurium during the annealing of BiSbTe thin films. An optimized Seebeck coefficient of 90.5 $\mu\text{V/K}$ along with a power factor of 240 $\mu\text{W/mK}^2$ is achieved for samples annealed at 350 °C for 1 h under N_2 atmosphere with controlled heating and cooling rates. These improvements are attributed to a significant decrease in the carrier concentration as substantiated by the Hall measurements and to the increase in the crystallite size at the elevated temperatures as indicated by the X-ray diffraction pattern data. A comprehensive study on the annealing parameters reveals that the Seebeck coefficient and the electrical conductivity are considerably more sensitive to the annealing temperature than compared to the annealing time.

© 2019 Author(s). All article content, except where otherwise noted, is licensed under a Creative Commons Attribution (CC BY) license (<http://creativecommons.org/licenses/by/4.0/>). <https://doi.org/10.1063/1.5049586>

Bismuth telluride based materials still dominate in thermoelectric (TE) properties for room temperature applications. Bulk materials have been extensively studied.^{1–3} However, they cannot be used in miniaturized thermoelectric devices due to integration and processing constraints. Thin film thermoelectric materials can be used for such applications.^{4–6} Various thin film deposition techniques have been reported, such as metal organic chemical vapour deposition (MOCVD),⁷ electrochemical deposition,⁸ molecular beam epitaxy (MBE),⁹ pulsed laser deposition,¹⁰ and thermal evaporation.¹¹ Among different deposition techniques, electrochemical deposition attracts attention due to its ease of deposition and industrial scalability.^{8,12} In addition, due to its selective deposition over a patterned structure, the wastage of material is minimized and hence becomes cost-effective. Also, the ability to tune material's stoichiometry makes the electrochemical technique potentially advantageous to be employed for the deposition of TE thin films. However, the TE properties, in particular, the

Seebeck coefficient of bulk materials are superior compared to the electrodeposited materials. This can be attributed to the high carrier concentrations of electrodeposited films in comparison to predicted carrier concentration by a common antistructure model.¹³ Various approaches, mainly using additives¹⁴ and doping,¹⁵ have been applied to enhance the TE properties of electrodeposited thin films. Annealing is an alternative route to further enhance the TE properties of electrochemically deposited thin films. Annealing passivates defects resulting in the decrease of structural and point defects and thereby reduces the defect density and the carrier concentration in the materials and, hence, improving the Seebeck coefficient.

Interdependent relation between the Seebeck coefficient, the carrier concentration, mobility, and the electrical conductivity can be expressed by these equations:

$$S = \frac{8\pi^2 k_b^2}{3eh^2} \cdot m^* T \left(\frac{\pi}{3n} \right)^{2/3}, \quad (1)$$

$$\frac{1}{\rho} = e \cdot n \cdot \mu, \quad (2)$$

where m^* is the effective mass, k_b is the Boltzmann constant, e is the electron charge, h is the Planck constant, n is the charge carrier concentration, μ is the mobility of charge carrier, ρ is the electrical resistivity, and T is the absolute temperature.¹ From the above relation, it can be seen that a decrease in the carrier concentration not only increases the Seebeck coefficient but also decreases the electrical conductivity. Therefore, an optimization is required, which in this work has been studied by optimizing the annealing parameters, namely, the annealing temperature-time profile.

The deposition of stoichiometric ternary BiSbTe alloy thin films is challenging compared to the binary material. One of the significant problems associated with the annealing of bismuth telluride alloy thin films is the evaporation of tellurium (Te) at elevated temperatures due to its high vapour pressure and thereby impacting on the composition and the TE properties of thin films.^{16,17} To circumvent the loss of Te during annealing and to maintain the film composition, they are usually annealed in the Te atmosphere for a long annealing time of about 60 h.¹⁸ This makes the process environmentally unfriendly, cumbersome, and industrially not scalable. Most of the annealing studies reported in the literature are on binary n-type bismuth telluride materials^{17,19–23} and few on p-type ternary material,¹⁸ but all are investigated in the Te atmosphere. Building-up on our previous work of using an encapsulated Te layer between the p-type BiSbTe film,¹⁶ here we study the effect of annealing parameters on the TE properties of electrodeposited p-type BiSbTe films. The experiments are performed at various annealing temperatures and times in the N₂ atmosphere. The impact of annealing temperature-time profile on the microstructure and TE properties is investigated in detail.

Thin films of p-type BiSbTe were deposited potentiostatically on a square (32 mm × 32 mm) Si/SiO₂ substrate, where a SiO₂ layer of 1 μm was thermally grown. On top of it, a titanium (Ti) layer of 10 nm and a gold (Au) layer of 20 nm were deposited, which act as a metal seed layer for electrochemical deposition. Depositions were performed at room temperature using the triple pulse amperometry technique in a three-electrode conventional setup. The electrodeposition potentials were controlled by a CHI600 series electrochemical analyser/work station. An Ag/AgCl reference electrode was used with a Pt mesh as a counter electrode. Prior to the deposition, all the substrates were cleaned with Isopropanol (IPA) and then with deionized (DI) water followed by drying with N₂ jet at ambient temperature.

Bismuth (III) nitrate pentahydrate (ACS reagent ≥98.0%), antimony (III) oxide, tellurium (powder × 200 mesh, 99.8% trace metals basis), tartaric acid (ACS reagent ≥99.5%), nitric acid (ACS reagent ≥69%), and dimethyl sulfoxide (DMSO) (ACS reagent ≥99.9%) were used for the experiments as received.

Dissolving Te powder and antimony oxide (Sb₂O₃) is nontrivial due to the surface TeO₂ that dissolves only in a strong HNO₃ medium and Sb₂O₃ having lower solubility in an

aqueous solution. Therefore, two separate solutions were made in order to dissolve the salts and combined at a later stage to form a stable electrolyte.

In preparing solution (A), 15 mM of Te was put into 25 ml of 1M HNO₃ and was heated at ~45 °C to dissolve Te completely and 5 mM Bi(NO₃)₃·5H₂O was added to the solution. Solution (B) was prepared using 10 mM Sb₂O₃ in 25 ml of 0.2M tartaric acid and was heated at ~45 °C for proper dissolution. Both solutions A and B were mixed, and 50 ml of dimethyl sulfoxide (DMSO) was added to the mixed solutions. The whole solution was maintained at 1:1 (v/v) ratio of DI water and DMSO.

In order to evaluate the reduction potential of the dissolved species, cyclic voltammetry (CV) studies were performed within the fixed potentials of −0.6 V and 0.8 V vs. Ag/AgCl at a scan rate of 10 mV/s. An optimised pulse design was used for deposition using the triple pulse amperometry technique for an overall duration of 2 h leading to two layers of BiSbTe films. The pure Te layer was deposited in between BiSbTe layers using an electrolyte with 15 mM Te in 1M nitric acid. The pulse deposition technique has various advantages over conventional potentiometric deposition such as uniform and adhesive films, low porosity, fine-grained structure, reduced surface roughness, improved morphology, and stoichiometry of the films.^{24–26} The overall deposition gave a film thickness of ~2 μm. Subsequently, the films were cleaned with IPA and DI water and dried under N₂ flow at ambient temperatures.

The structural characterization of thin films was performed using a scanning electron microscopy (SEM), and the composition was determined with energy dispersive X-ray (EDX) spectroscopy attached to the SEM. All the SEM analyses were performed on the Quanta Field emission gun (FEG) 450 at an accelerating voltage of 20 kV at 20 Kx magnification. X-ray diffraction (XRD) patterns were recorded using a Pan analytical X'pert pro, with Cu K_α radiation ($\lambda = 1.5406 \text{ \AA}$) at a voltage of 40 kV and a current of 40 mA. Electrical resistivity and Hall measurements were performed using an inline four-point probe measurement system (Jandel RM300) and in Hall arrangement for the Hall coefficient (Lakeshore model 8404) to independently measure the sheet resistivity of the samples. The Seebeck coefficient of the electrodeposited thin films was measured using a laboratory built system.

The Seebeck coefficient for all samples was evaluated in the in-plane configuration by establishing a temperature gradient (ΔT) along the length of the sample through commercially available thermoelectric coolers at the two ends of the sample. The thermovoltage was measured in the range of $\Delta T \approx 2\text{--}10 \text{ }^\circ\text{C}$. Two separate thermocouples situated at the ends of the sample recorded the temperatures. The Seebeck coefficient was evaluated from the slope of the thermovoltage against ΔT . The Seebeck coefficient was calculated with the intact seed layer.

The thermal treatment of the electrodeposited films was performed under the controlled flow of N₂ atmosphere in a rapid thermal annealing (RTA) system for a different time duration ranging from 15 min to 1 h and at different

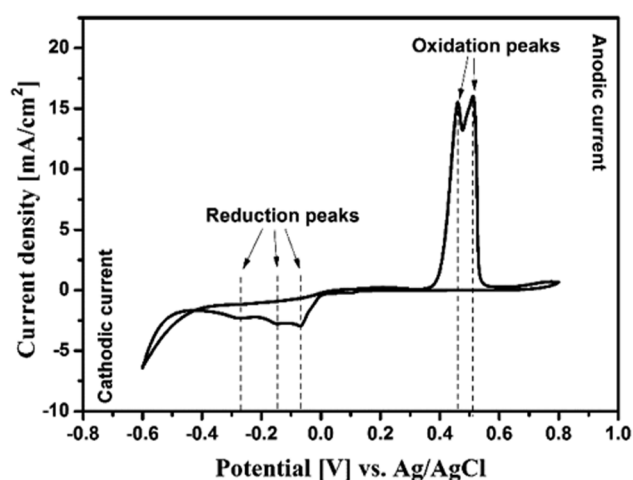
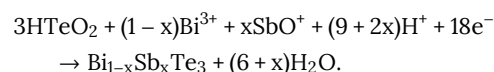


FIG. 1. Cyclic voltammogram recorded on a gold working electrode in the electrolyte containing 0.005M Bi^{3+} , 0.010M SbO^+ , 0.015M HTeO^+ , and 1M HNO_3 . The CV's are recorded at room temperature at a scan rate of 10 mV/s.

temperatures ranging from 250–400 °C. The samples were heated from room temperature to the desired annealing temperature in a controlled heating and cooling rate of 20 K/min and kept at that temperature for set time duration. Three sets of samples were prepared to ensure the reproducibility of the properties.

The deposition mechanism of ternary alloys from the electrolytic bath solution is more complex than the deposition of binary materials. Thus, fine optimization of plating parameters is required for controlled film composition. The electrolyte constitutes with Bi^{3+} , SbO^+ , and HTeO^+ ions.²⁷ In order to understand the deposition potentials of the constituents, cyclic voltammograms (CVs) were recorded, using a standard Au working electrode of 1 mm radius and with a scan rate of

10 mV/s. As shown in Fig. 1, CV reveals three cathodic peak potentials at -0.07, -0.15, and -0.27 V vs. Ag/AgCl and two anodic peaks at 0.46 and 0.51 V vs. Ag/AgCl. These reduction peaks can be attributed to Bi, Te, and Sb, respectively.²⁸ The deposition of the desired composition of $(\text{Bi}_{1-x}\text{Sb}_x)\text{Te}_3$ can be described as²⁰



Based on the CV studies, the deposition potentials were fixed as optimized in our previous work.¹⁴ Triple pulse amperometry was used at potentials $V_1 = -80$ mV for a duration of 10 ms, $V_2 = -50$ mV for a duration of 20 ms, and $V_3 = -250$ mV for a duration of 50 ms. The films were deposited for a duration of 2 h in order to attain a thickness of 2 μm .

Due to the high vapour pressure of Te and considerable evaporation at elevated temperatures, these samples were annealed in the temperature range of 250–400 °C with a step of 50 °C for the time duration of 1 h. In order to understand the effect of annealing temperature on the microstructure, micrographs were recorded using SEM. Figure 2 shows the micrograph of as-deposited and annealed films. The microstructures of the films changed drastically with the increasing annealing temperatures. The dendritic and fluffy structure of the as-deposited films collapses as the annealing temperature is increased and gets modified to dense films. At the high annealing temperature of 350 °C and 400 °C, we observed a porous network in the films, which is due to the loss of Te at these temperatures. In order to understand the effect of thermal treatment on these films, the composition was analyzed using EDX analysis and is depicted in Table I. It is interesting to observe that, there has been no significant change in the composition of the films on annealing even though there has been a strong modification in the microstructure. This observation can be ascribed to the depletion of excess Te that is

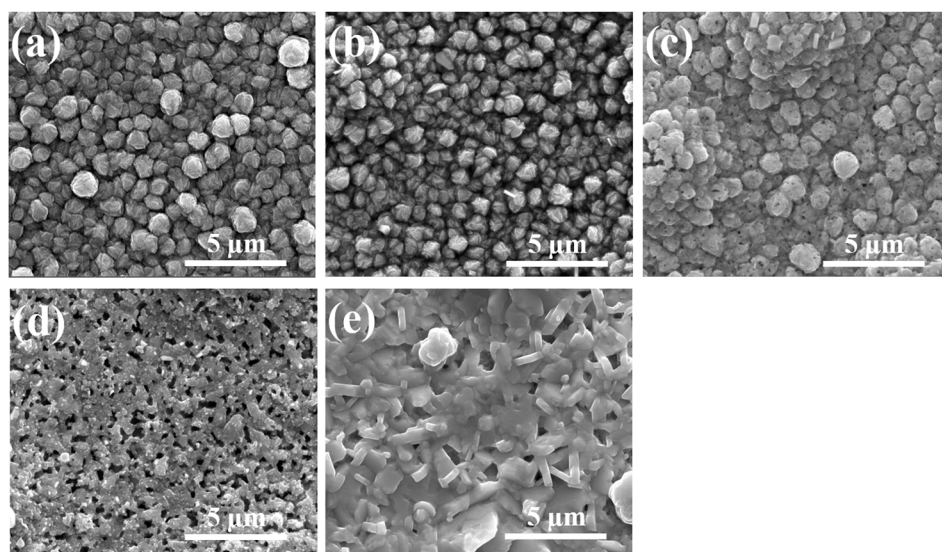


FIG. 2. SEM images of (a) as-deposited samples and samples annealed at (b) 250 °C, (c) 300 °C, (d) 350 °C, and (e) 400 °C.

TABLE I. Atomic composition of Bi-Sb-Te as-deposited films and films annealed at different annealing temperatures.

Annealing temperature (°C)	Film composition (at. %)		
	Sb	Te	Bi
As-deposited	24.05	60.11	15.84
250	24.10	59.69	16.21
300	24.69	58.96	16.35
350	23.36	59.68	16.96
400	21.86	60.04	18.13

sandwiched between the *p*-BiSbTe layer during annealing and thereby resulting in the stoichiometric films.

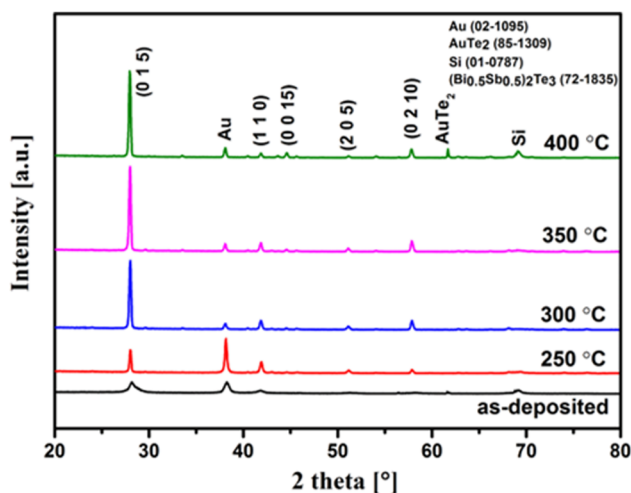
Figure 3 shows the XRD patterns of the as-deposited and the films annealed at different temperatures. Standard references for $(\text{Sb}_{0.5}\text{Bi}_{0.5})_2\text{Te}_3$, Au, AuTe_2 , Si are obtained from the inorganic crystal structure database (ICSD) powder diffraction file (PDF) card (72-1835, 02-1095, 85-1309, 01-0787), respectively. All the films have a rhombohedral crystal structure of $(\text{Sb}_{1-x}\text{Bi}_x)_2\text{Te}_3$, with (015) being the prominent peak. However, some small peaks with different orientation were observed after annealing at different temperatures. An AuTe_2 peak was observed for the films annealed at 400 °C, indicating the formation of a new phase due to the diffusion and reaction of Te with Au, forming AuTe_2 . The Au and Si peak observed in the XRD patterns are from the seed layer. The average crystallite size was calculated using the Debye-Scherrer formula and presented in Table II. There is a significant increase in the crystallite size of annealed films as compared to as-deposited films (see Table II). The size increases as the annealing temperature is raised to 250 °C. After that, there has been little or no change in the crystallite size. However, it was observed that with increasing annealing temperature, the intensity of (015) peak increases, thereby signifying a preferred growth along (015) orientation in the film. (see Fig. 3). Also, the micrographs

TABLE II. Crystallite size of films annealed at different annealing temperatures.

Annealing temperature (°C)	Crystallite size (nm)
As-deposited	11.55
250	37.20
300	35.61
325	35.61
350	37.16
375	37.16
400	35.61

reveal that the grain size increases with the increasing annealing temperature as shown in Fig. 2. The annealed films tend to form large and dense grains with increased connectivity in-between the grains. This can be attributed to the change in the crystallite size between the as-deposited and annealed films.

Thermoelectric properties, namely, the Seebeck coefficient, the electrical conductivity, and the power factor were measured and calculated for the as-deposited and annealed samples at different temperatures as shown in Figs. 4(a) and 4(b). The Seebeck coefficient of films increased with the annealing temperatures, and the maximum Seebeck coefficient was observed for the samples annealed at 350 °C. On further increment of the temperature, the Seebeck coefficient of the film decreased. The electrical conductivity of the as-deposited films is an order of magnitude higher compared to the annealed film. In-order to understand this, Hall measurements of the films were performed. Figure 5 shows the Hall measurements of the as-deposited and annealed samples. The carrier concentration of the as-deposited film is 1.58×10^{21} carrier/cm³, which is more than an order of magnitude higher compared to the annealed films, which is around $2-6 \times 10^{19}$ carriers/cm³ (see Fig. 5). This reduction in the carrier concentration of the annealed films resulted in reduced electrical conductivity and a simultaneous increase in the Seebeck coefficient. The mobility of the as-deposited films is measured to be 8.9 cm²/V s, which increased upon annealing of films. This increase in the mobility of charge carriers with the annealing can be interrelated to the structural transformations as revealed through micrographs in Fig. 2. With annealing, the films become denser and get connected to adjacent grains, and as an outcome, the mobility of the annealed films increases, as shown in Fig. 5. In addition, with annealing, crystallinity of thin films was improved resulting in an increase in the average grain size and minimization of grain boundaries that leads to higher mobility. The mobility of the charge carriers is observed to increase with the annealing temperature from ~30 cm²/V s for the film annealed at 250 °C to ~125 cm²/V s for films annealed at 400 °C. A slight drop in the mobility of charge carriers is observed for films annealed at 350 °C, and this reduction may be due to the porosity in the film, resulted from the Te evaporation [see Fig. 2(d)]. Upon further increase in the temperature, the microstructure further collapses and becomes dense forming interconnected grains; this led to an increase in the mobility [Fig. 2(e)]. This increase in the mobility and no drastic changes in the carrier concentration for the annealed films have led to a gradual and

**FIG. 3.** XRD patterns of the as-deposited and the annealed BiSbTe films. The annealing temperatures are mentioned in the pattern.

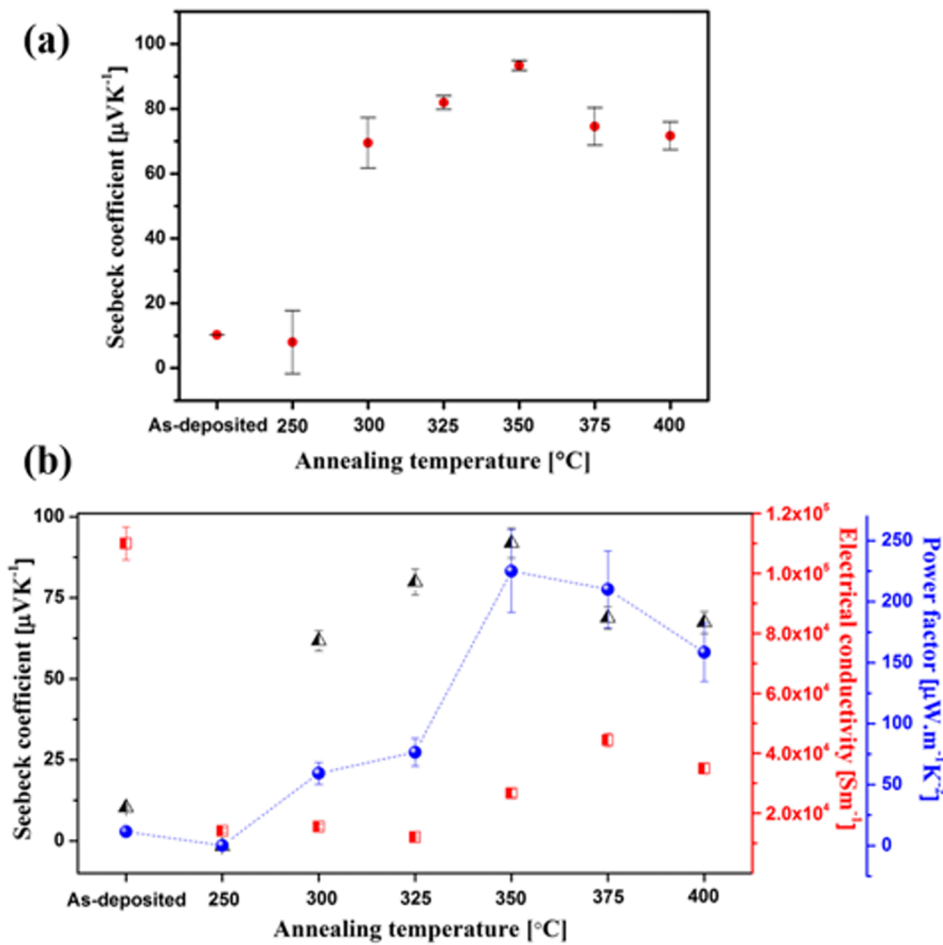


FIG. 4. (a) Seebeck coefficient of BiSbTe films annealed at different temperatures for 1 h with the error bars. (b) Seebeck coefficient, electrical conductivity, and calculated power-factor of as-deposited and annealed films.

slight increment in the electrical conductivity of the annealed films from 250 $^\circ\text{C}$ –400 $^\circ\text{C}$. The electrical conductivities of the films were measured using the in-line four-point probe

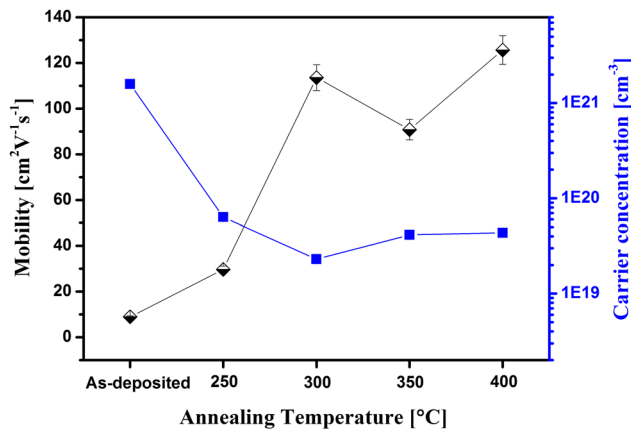


FIG. 5. Carrier mobility and carrier concentration of BiSbTe thin films as a function of the annealing temperature.

measurement system, which was also used to cross-check the conductivity values obtained from the Hall measurements. The values from both the measurement techniques are almost the same, ensuring that the obtained data are correct and are within the error limits of the measurements. As stated earlier, three different set of samples were deposited and annealed. The variation in their Seebeck coefficient values are plotted with error bars in Fig. 4(a). It can be noticed from the figure that the error bars depict the spread in the measured Seebeck coefficient values, which reduce and become significantly low at around 350 $^\circ\text{C}$ showing higher stability in the Seebeck coefficient values for 350 $^\circ\text{C}$ annealed thin films.

The power factor of all the films was calculated and plotted as shown in Fig. 4(b). The power factor of the as-deposited films was 11 $\mu\text{W/mK}^2$, which increased for the annealed films, and a maximum power factor of 225 $\mu\text{W/mK}^2$ was obtained for the films annealed at 350 $^\circ\text{C}$ for a duration of 1 h in N_2 atmosphere. The power factor of the annealed films increased due to the increment in both the Seebeck coefficient and the electrical conductivity of the annealed films. This shows the role of annealing parameters in fine-tuning the

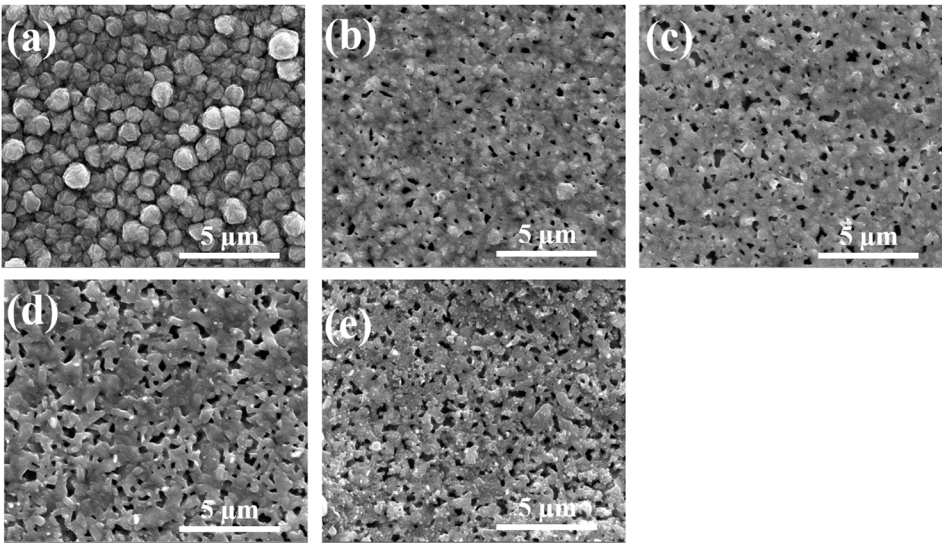


FIG. 6. SEM images of (a) as-deposited samples and samples annealed at 350 °C for a duration of (b) 15 min, (c) 30 min, (d) 45 min, and (e) 60 min.

individual thermoelectric properties of the electrodeposited films.

To further understand the effect of annealing time on the TE performance of the films, samples were annealed at 350 °C for different duration of time from 15 min to 1 h. The 350 °C annealing temperature was chosen for further analysis as the maximum power factor was attained at this temperature. Figure 6 shows the micrographs of films annealed for different annealing times. From the micrographs, it can be observed that there is no specific change in the microstructure of the films annealed for different duration of time except the porosity of the films, which tends to increase with increasing annealing times. The as-deposited films are dendritic and fluffy in nature, which on annealing at 350 °C for 15 min become granulated and crystalline, but a porous network appears at the same time. The porosity in the films is increased with increasing annealing time from 15 min to 1 h. Even though an increase in the porosity is observed, which can be attributed to the Te evaporation, the composition of all the films has no significant change as tabulated in Table III. This can be ascribed to the sandwich Te layer in the films, which replenishes Te content during annealing of the films.

To understand the impact of annealing time on the crystallinity of the films, the XRD patterns were recorded for

the films with increasing time of thermal treatment. Figure 7 shows the XRD patterns of the as-deposited films and films annealed with annealing time varied from 15 to 60 min. Table IV shows the calculated average crystallite size of different films. All the films had (015) peak as the prominent peak similar to earlier samples with different annealing temperatures. In comparison with the as-deposited sample, the (015) peak for the annealed film is sharp and higher in intensity with the increase in the crystallite size. The emergence of other small peaks confirms that the annealed films are polycrystalline. The Au peak observed in the XRD patterns is from the seed layer. It is noteworthy to mention that the crystallite size of the as-deposited films was 11.55 nm, which on annealing at 350 °C for 15 min increased to 38.85 nm. But further increase

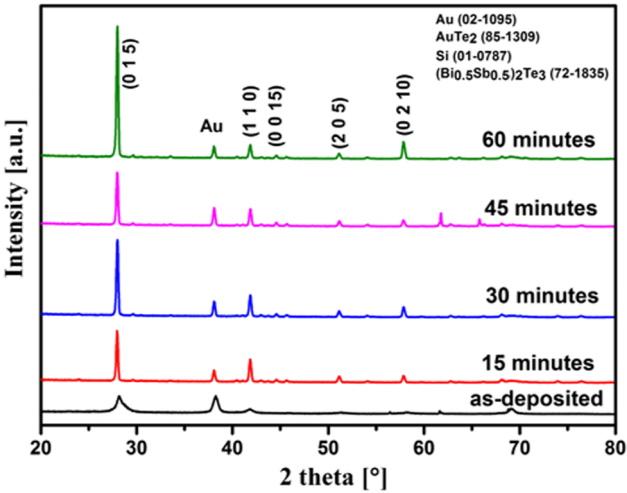


FIG. 7. XRD patterns of BiSbTe films annealed at 350 °C for different annealing time.

TABLE III. Atomic composition of Bi–Sb–Te as-deposited films and films annealed at 350 °C for different annealing time.

Annealing time (min)	Film composition (at. %)		
	Sb	Te	Bi
As-deposited	24.05	60.11	15.84
15	22.91	59.87	17.21
30	22.95	59.40	17.14
45	23.17	59.48	17.34
60	23.36	59.68	16.96

TABLE IV. Crystallite size of films annealed at 350 °C for different annealing time.

Annealing time (min)	Crystallite size (nm)
As-deposited	11.55
15	38.85
30	37.16
45	37.16
60	37.16

in the annealing time had no significant effect on the crystallite size. However, from the micrographs, it can be seen that the grain-size tends to enhance with increasing annealing time and also made the films more porous. This shows that the duration of annealing has no noticeable effect on the crystallite size of the material and the temperature of annealing controls the crystallite size.

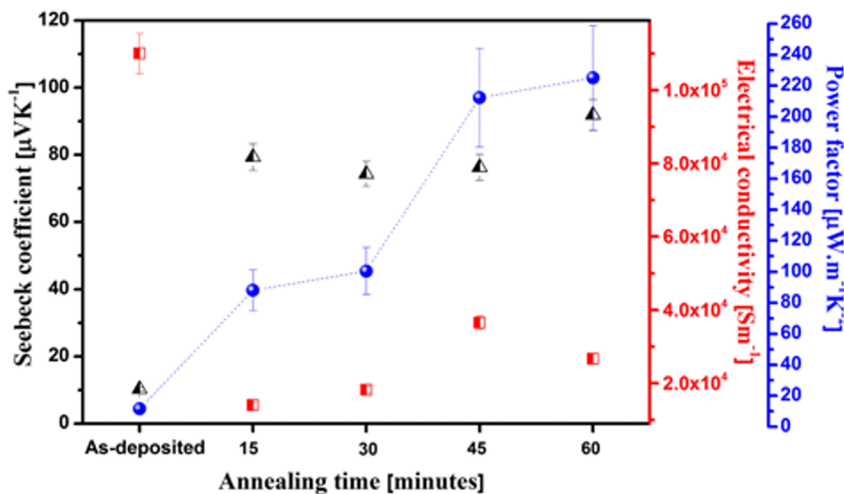
The Seebeck coefficient and the electrical conductivity were measured for the as-deposited film and the films annealed at 350 °C for different duration of time and plotted as shown in Fig. 8. The Seebeck coefficient of the annealed films varied slightly with increasing annealing time, whereas the electrical conductivity exhibits an optimum for films annealed for 45 min as seen in Fig. 8. In order to understand this change in the Seebeck coefficient and the electrical conductivity, the Hall study was performed on the samples and the results are plotted in Fig. 9.

The carrier concentration of the annealed films compared to as-deposited films reduced by more than an order of magnitude as discussed earlier in this work. It is noticeable that even a small change in the carrier concentration of the annealed films is directly reflected in the change of measured Seebeck coefficient. The Seebeck coefficient of the film annealed at 350 °C for 15 min was 79.3 $\mu\text{V/K}$, which increased to 90.5 $\mu\text{V/K}$ for the film annealed for 1 h. Although the change is not significant but when coupled with the electrical conductivity of film, it has a strong impact on the power factor of the films. The increase in the mobility from 8.9 $\text{cm}^2/\text{V s}$ for the as-deposited film to 90.7 $\text{cm}^2/\text{V s}$ for films annealed at

350 °C for 1 h had an impact on increasing the electrical conductivity of the films. With the increase in annealing time from 15 min to 1 h, the mobility of the charge carriers increased even though there was no significant change in the carrier concentration. This insignificant change in the carrier concentration of the films with increasing annealing time might be due to the fact that the defect density stabilization has already reached at this particular temperature, and increasing the annealing time only changes the microstructure further with better grain connectivity. This leads to an increase in the mobility as shown in Fig. 9 and consequently an increase in the electrical conductivity as shown in Fig. 8. This increase in the electrical conductivity of the annealed films with no significant change in the carrier concentration led to an increase in the overall power factor of the films, giving a maximum power factor of 225 $\mu\text{W/mK}^2$ for the film annealed for 1 h at 350 °C.

This study signifies the importance of annealing parameters, such as temperature and time, on the thermoelectric properties of electrodeposited p-type BiSbTe films. The inclusion of a Te layer in-between BiSbTe layers prevents the loss of tellurium at elevated temperatures maintaining the stoichiometry of the deposited films regardless of the annealing conditions.

The microstructure evaluation studies depict the densification and interconnected nature of the films with different annealing parameters. It demonstrates the control over the carrier concentration and the mobility by tuning the annealing parameters. The Seebeck coefficient values of the annealed films increase with the annealing temperature leading to an optimum value of 90.5 $\mu\text{V/K}$ when annealed at 350 °C for 1 h duration in N_2 atmosphere under controlled heating and cooling rates. The maximum power factor of 225 $\mu\text{W/mK}^2$ is achieved for the same annealing conditions as above but decreases beyond that temperature. No substantial change in the Seebeck coefficient is observed with increasing annealing time. However, due to an increase in the mobility of the carriers with increasing annealing time, the electrical conductivity gradually rises. This result in a maximum power factor for thin films annealed for 1 h.

**FIG. 8.** Thermoelectric properties of BiSbTe films annealed at 350 °C for different annealing times.

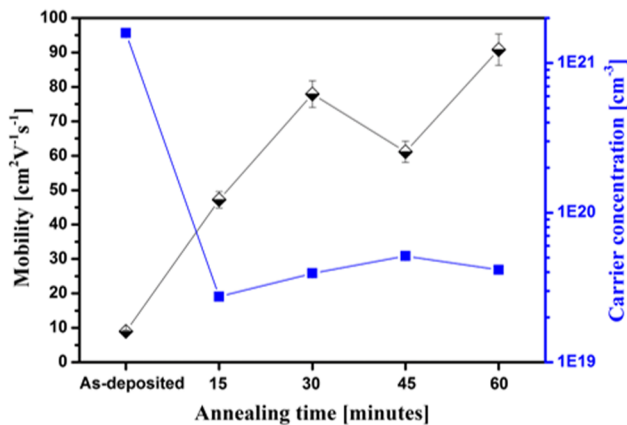


FIG. 9. Mobility and carrier concentration as a function of the annealing time of BiSbTe films annealed at 350 °C.

This work has received funding from the European Union's Horizon 2020 funded project "Thermally Integrated Smart Photonics Systems (TIPS)", under the Grant Agreement No. 644453, and Science Foundation Ireland (SFI) under Grant No. 15/IA/3160. This publication has emanated from research supported in part by a research grant from Science Foundation Ireland (SFI) and is co-funded under the European Regional Development Fund under Grant Number 13/RC/2077. One of the authors (D.G) acknowledges Science Foundation Industry Fellowship (grant agreement SFI-16/IFB/4587) to carry out the present work.

REFERENCES

- G. J. Snyder and E. S. Toberer, *Nat. Mater.* **7**(2), 105–114 (2008).
- J. He, M. G. Kanatzidis, and V. P. Dravid, *Mater. Today* **16**(5), 166–176 (2013).
- L.-D. Zhao, V. P. Dravid, and M. G. Kanatzidis, *Energy Environ. Sci.* **7**(1), 251–268 (2014).
- L. E. Bell, *Science* **321**(5895), 1457–1461 (2008).
- R. Venkatasubramanian, *Nature* **413**, 597–602 (2001).
- B. Habbe and J. Nurnus, *Electron. Cool.* **17**, 24–31 (2011).
- A. Giani, A. Boulouz, F. Pascal-Delannoy, A. Foucaran, E. Charles, and A. Boyer, *Mater. Sci. Eng. B: Solid-State Mater. Adv. Technol.* **64**(1), 19–24 (1999).
- C. Boulanger, *J. Electron. Mater.* **39**(9), 1818–1827 (2010).
- T. C. Harman, P. J. Taylor, M. P. Walsh, and B. E. LaForge, *Science* **297**(5590), 2229–2232 (2002).
- A. Li Bassi, A. Bailini, C. S. Casari, F. Donati, A. Mantegazza, M. Passoni, V. Russo, and C. E. Bottani, *J. Appl. Phys.* **105**(12), 124307 (2009).
- J.-M. Lin, Y.-C. Chen, and C.-P. Lin, *J. Nanomater.* **2013**, 6.
- F. Xiao, C. Hangarter, B. Yoo, Y. Rheem, K.-H. Lee, and N. V. Myung, *Electrochim. Acta* **53**(28), 8103–8117 (2008).
- K. Tittes, A. Bund, W. Plieth, A. Bentien, S. Paschen, M. Plötner, H. Gräfe, and W.-J. Fischer, *J. Solid State Electrochem.* **7**(10), 714–723 (2003).
- S. Lal, D. Gautam, and K. M. Razeed, *ECS J. Solid State Sci. Technol.* **6**(3), N3017–N3021 (2017).
- R. Rostek, N. Stein, and C. Boulanger, *J. Mater. Res.* **30**(17), 2518–2543 (2015).
- K. M. Razeed and D. Gautam, U.S. patent 2017/010414.6 A1 (13 April 2017).
- R. Rostek, V. Sklyarenko, and P. Woias, *J. Mater. Res.* **26**(15), 1785–1790 (2011).
- C. Schumacher, K. G. Reinsberg, R. Rostek, L. Akinsinde, S. Baessler, S. Zastrow, G. Rampelberg, P. Woias, C. Detavernier, J. A. C. Broekaert, J. Bachmann, and K. Nielsch, *Adv. Energy Mater.* **3**(1), 95–104 (2013).
- N. G. Stoltz and G. J. Snyder, in *Proceedings of the Twenty-First International Conference on Thermoelectrics, ICT'02* (IEEE, 2002), pp. 28–30.
- S. Li, H. M. A. Soliman, J. Zhou, M. S. Toprak, M. Muhammed, D. Platzek, P. Ziolkowski, and E. Müller, *Chem. Mater.* **20**(13), 4403–4410 (2008).
- M. M. Rashid, K. H. Cho, and G.-S. Chung, *Appl. Surf. Sci.* **279**, 23–30 (2013).
- D. M. Lee, C. H. Lim, D. C. Cho, Y. S. Lee, and C. H. Lee, *J. Electron. Mater.* **35**(2), 360 (2006).
- S. Kamolmad, S. Aparporn, and S. Rachsak, *Adv. Nat. Sci.: Nanosci. Nanotechnol.* **8**(3), 035002 (2017).
- V. Richoux, S. Diliberto, and C. Boulanger, *J. Electron. Mater.* **39**(9), 1914–1919 (2010).
- V. Richoux, S. Diliberto, C. Boulanger, and J. M. Lecuire, *Electrochim. Acta* **52**(9), 3053–3060 (2007).
- S. Diliberto, V. Richoux, N. Stein, and C. Boulanger, *Phys. Status Solidi A* **205**(10), 2340–2344 (2008).
- X. Li, E. Koukharenko, I. S. Nandhakumar, J. Tudor, S. P. Beeby, and N. M. White, *Phys. Chem. Chem. Phys.* **11**(18), 3584–3590 (2009).
- J. Kuleshova, E. Koukharenko, X. Li, N. Frety, I. S. Nandhakumar, J. Tudor, S. P. Beeby, and N. M. White, *Langmuir* **26**(22), 16980–16985 (2010).